Takuma Yamashita (ID) · **Yasushi Kino** · **Emiko Hiyama** · **Svante Jonsell** · **Piotr Froelich**

Four-body Calculation of Inelastic Scattering Cross Sections of Positronium–Antihydrogen Collision

Abstract We overview our recent calculations of scattering cross sections of positronium–antihydrogen collisions. We discuss the cross sections calculated in the vicinity of the four-body resonances of $\bar{\text{H}}$Ps and above the energy threshold for the formation of the antihydrogen positive ions ($\bar{\text{H}}^+$). In the former energy region where a Rydberg series of resonances dominated by the $\bar{\text{H}}^+$-e^- interaction appears, we show a good agreement between the resonant profiles in the cross sections and the resonance energies calculated by the complex coordinate rotation method. $\bar{\text{H}}^+$ production cross sections near the threshold energy are reported for the positronium being initially in the (n, l) states with $n \leq 3$, together with all competing elastic/inelastic cross sections. Comparison of our results with the latest continuum distorted wave final state calculation is presented. A qualitative discrepancy concerning the dependence of cross sections on the angular momentum of Ps is indicated.

1 Introduction

The simplest antiatom, antihydrogen ($\bar{\text{H}}$), consisting of an antiproton ($\bar{\text{p}}$) and a positron (e^+) can be a probe of fundamental physics. So far the development of $\bar{\text{H}}$ production [1–7] has been mainly focused on antihydrogen spectroscopy with particular emphasis on a test of CPT symmetry [8–11].

T. Yamashita (✉)
Institute for Excellence in Higher Education, Tohoku University, Sendai, Miyagi 980-8576, Japan

T. Yamashita · Y. Kino
Department of Chemistry, Tohoku University, Sendai, Miyagi 980-8578, Japan
E-mail: tyamashita@tohoku.ac.jp

E. Hiyama
Department of Physics, Tohoku University, Sendai, Miyagi 980-8578, Japan

E. Hiyama
Nishina Center, RIKEN, Wako, Saitama 351-0198, Japan

S. Jonsell
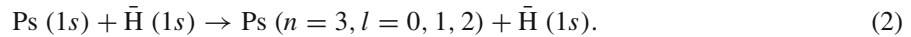Department of Physics, Stockholm University, 10691 Stockholm, Sweden

P. Froelich
Department of Chemistry, Uppsala University, Box 518, 751-20 Uppsala, Sweden

Since the $\bar{\text{H}}$ is an electrically neutral system purely consisting of antiparticles, it can be a probe of the gravitational interaction between matter and antimatter [12–23]. In the GBAR project [14–17], the ultra-cold $\bar{\text{H}}$ for free-fall experiments is to be obtained via sympathetic cooling of antihydrogen ions ($\bar{\text{H}}^+ = \bar{\text{p}}\text{e}^+\text{e}^+$) and the subsequent positron photodetachment. The $\bar{\text{H}}^+$ ions are to be obtained in collisions of positronium (Ps = e^-e^+) and $\bar{\text{H}}$.

In a collision between Ps($1s$) and $\bar{\text{H}}(1s)$, the first excitation channels of Ps open at the collision energy 5.1 eV,

$$\text{Ps}\,(1s) + \bar{\text{H}}\,(1s) \to \text{Ps}\,(n = 2, l = 0, 1) + \bar{\text{H}}\,(1s), \tag{1}$$
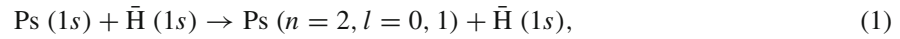
and the next excitation channels of Ps open at 6.0469 eV,

$$\text{Ps}\,(1s) + \bar{\text{H}}\,(1s) \to \text{Ps}\,(n = 3, l = 0, 1, 2) + \bar{\text{H}}\,(1s). \tag{2}$$

The $\bar{\text{H}}^+$ production channel,

$$\text{Ps}\,(1s) + \bar{\text{H}}\,(1s) \to \text{e}^- + \bar{\text{H}}^+, \tag{3}$$

opens at the threshold energy 6.0486 eV, just above the Ps second excitation threshold energy. Owing to the parity conservation and the fact that $\bar{\text{H}}^+$ bound state is allowed only for the spin singlet positrons, under LS-coupling approximation, the $\bar{\text{H}}^+$ production channel does not open when the two positrons form spin triplet.

Due to the charge-conjugation symmetry, Ps + $\bar{\text{H}}$ collisions are equivalent to Ps + H collisions. Low-energy scattering of Ps($1s$) and H has been studied as a fundamental example of positronium-atom interaction [24–28], and elastic scattering cross sections for collision energies below 5.1 eV and scattering lengths have been accurately obtained [29–39]. In recent years, the Ps collisions with atoms/molecules at low energies attract attentions with particular focus on the correspondence between the experiments [40] and theories [28,41–43].

The understanding of inelastic scattering including the $\bar{\text{H}}^+$ formation, however, has been limited. The reaction has a multichannel nature due to the presence of the fragmentation channels of Ps ($n \le 3$) + $\bar{\text{H}}$ ($1s$), and the $\bar{\text{H}}^+$ production reaction is a rearrangement process where the particle configuration drastically changes from initial channel to final channel, which requires a simultaneous treatment of all constituent particles and does not allow the semi-classical approximations. Even below the threshold energy of $\bar{\text{H}}^+$ production, a resonant scattering involving $\bar{\text{H}}^+$ formation occurs:

$$\text{Ps}(1s) + \bar{\text{H}}(1s) \to [\text{e}^-; \bar{\text{H}}^+] \to \text{Ps}(n \le 2) + \bar{\text{H}}(1s), \tag{4}$$
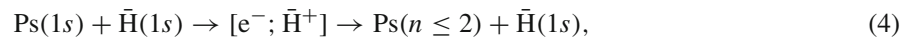
where $[\text{e}^-; \bar{\text{H}}^+]$ is a resonance state having an electron attached to $\bar{\text{H}}^+$ core.

So far, the Born-based approximations and eikonal-based approximations have been adopted to predict $\bar{\text{H}}^+$ production cross sections; however, such approximations assume intermediate to high energy collisions, and may not be appropriate for low-energy scattering. In fact, the $\bar{\text{H}}^+$ production cross section in Ps($1s$) + $\bar{\text{H}}(1s)$ collision just above the threshold energy differs by more than one order of magnitude in the first Born approximation (FBA) [44], the distorted wave Born approximation (DWBA) [44], and the Coulomb-modified eikonal approximation (CMEA) [45]. We recently reported a rigorous four-body treatment of Ps-$\bar{\text{H}}$ scattering [46,47] utilizing a Gaussian expansion method (GEM) and also calculated the $\bar{\text{H}}^+$ production cross sections above its threshold energy [48,49]. Very recently, a continuum distorted wave final state (CDW-FS) calculation was updated with corrections in its implementation [50–53]. Since the CDW-FS involves perturbative nature of the formulation, the suitability of this approach to the near-threshold production of $\bar{\text{H}}^+$ remains to be tested by more rigorous calculations.

In this paper, we review our recent four-body scattering calculations of Ps-$\bar{\text{H}}$ collisions and compare with the latest CDW-FS calculations. This paper is organized as follows. In Sect. 2, we show outline of our calculation. In Sect. 3, the inelastic scattering cross sections above the first excitation threshold energy of Ps are displayed. Subsequently, $\bar{\text{H}}^+$ production cross sections from various Ps states ($1s$, $2s$, $2p$, $3s$, $3p$, $3d$) are compared with the competing inelastic scattering cross sections and with the CDW-FS results. We conclude our investigation in Sect. 4. Atomic units (a.u.; $m_\text{e} = \hbar = e = 1$) are used throughout this paper, except where mentioned otherwise.

Table 1 Definition of arrangement channels $\mathcal{F}$ and the detailed channels α

$\mathcal{F}$	Fragments	$J = 0$	$J = 1$	$J = 2$	$J = 3$
1	$\mathrm{Ps}(1s) + \bar{\mathrm{H}}(1s)$	$\lambda = 0: \alpha = 1$	$\lambda = 1: \alpha = 1$	$\lambda = 2: \alpha = 1$	$\lambda = 3: \alpha = 1$
2	$\mathrm{Ps}(2s) + \bar{\mathrm{H}}(1s)$	$\lambda = 0: \alpha = 2$	$\lambda = 1: \alpha = 2$	$\lambda = 2: \alpha = 2$	$\lambda = 3: \alpha = 2$
3	$\mathrm{Ps}(2p) + \bar{\mathrm{H}}(1s)$	$\lambda = 1: \alpha = 3$	$\lambda = 0: \alpha = 3$	$\lambda = 1: \alpha = 3$	$\lambda = 2: \alpha = 3$
			$\lambda = 2: \alpha = 4$	$\lambda = 3: \alpha = 4$	$\lambda = 4: \alpha = 4$
4	$\mathrm{Ps}(3s) + \bar{\mathrm{H}}(1s)$	$\lambda = 0: \alpha = 4$	$\lambda = 1: \alpha = 5$	$\lambda = 2: \alpha = 5$	$\lambda = 3: \alpha = 5$
5	$\mathrm{Ps}(3p) + \bar{\mathrm{H}}(1s)$	$\lambda = 1: \alpha = 5$	$\lambda = 0: \alpha = 6$	$\lambda = 1: \alpha = 6$	$\lambda = 2: \alpha = 6$
			$\lambda = 2: \alpha = 7$	$\lambda = 3: \alpha = 7$	$\lambda = 4: \alpha = 7$
6	$\mathrm{Ps}(3d) + \bar{\mathrm{H}}(1s)$	$\lambda = 2: \alpha = 6$	$\lambda = 1: \alpha = 8$	$\lambda = 0: \alpha = 8$	$\lambda = 1: \alpha = 8$
			$\lambda = 3: \alpha = 9$	$\lambda = 2: \alpha = 9$	$\lambda = 3: \alpha = 9$
				$\lambda = 4: \alpha = 10$	$\lambda = 5: \alpha = 10$
7	$\mathrm{e}^{-} + \bar{\mathrm{H}}^{+}$	$\lambda = 0: \alpha = 7$	$\lambda = 1: \alpha = 10$	$\lambda = 2: \alpha = 11$	$\lambda = 3: \alpha = 11$

λ denotes the angular momentum of relative motion of the fragments. We list only the channels that can lead to rearrangement reaction

2 Theory

We briefly describe the calculation framework and definitions of cross sections in this section. A more detailed description of the theoretical framework can be found in our previous papers [46–49].

We consider the Schrödinger equation for the non-relativistic time-independent scattering wavefunction [54],

$$(H - E)\Psi = 0, \tag{5}$$

where the Hamiltonian H includes kinetic energy operators in center-of-mass frame and all inter-particle Coulomb potential operators. We construct the total wavefunction Ψ as

$$\Psi = \sum_{\alpha} \psi_{\alpha} + \sum_{\upsilon=1}^{\upsilon_{\max}} b_{\upsilon} \Phi_{\upsilon} \tag{6}$$

where ψ_{α} are open channel functions that describe the asymptotically non-vanishing component and Φ_{υ} are square-integrable four-body eigenfunctions that diagonalize the Hamiltonian in the matrix form and satisfy

$$\langle \Phi_{\upsilon'} | H | \Phi_{\upsilon} \rangle = E_{\upsilon} \delta_{\upsilon' \upsilon}. \tag{7}$$

Here, E_{υ} is the υ-th eigenenergy.

In order to give a definition of open channel α, we consider the parity P and a total orbital angular momentum J. Throughout this paper, only spin-independent interactions are considered; therefore, J and P are conserved and stay the same both in the initial and final channels. In collisions between $\mathrm{Ps}(n_i l_i)$ and $\bar{\mathrm{H}}(N_i L_i)$, the total orbital angular momentum is given as $\mathbf{J} = \mathbf{l}_i + \mathbf{L}_i + \boldsymbol{\lambda}_i$ where λ_i is an angular momentum of relative motion. The parity of the spatial part of ψ_{α} is given by $P_i = (-1)^{l_i + L_i + \lambda_i}$.

Considering $L = 0$ case and the final channel of the Ps excitation scattering that results in $\mathrm{Ps}(nl) + \bar{\mathrm{H}}(1s)$ in λ-wave, $|l - \lambda| \leq J \leq l + \lambda$ and $P = (-1)^{l+0+\lambda} = (-1)^{l_i+0+\lambda_i} = P_i$ should be satisfied. Besides, in the final channel of the rearrangement process, the ground state of $\bar{\mathrm{H}}^{+}(^1S^e)$ possesses the total orbital angular momentum $\mathcal{L} = 0$. As a consequence, the spatial part of its wavefunction has positive parity. In the final channel of $\mathrm{e}^{-} + \bar{\mathrm{H}}^{+}$, denoting the angular momentum of relative motion λ, the total orbital angular momentum becomes $|\lambda - \mathcal{L}| \leq J \leq \lambda + \mathcal{L}$ (hence $J = \lambda$ for $\mathcal{L} = 0$) and the parity is $P = (-1)^{\lambda + \mathcal{L}} = (-1)^{J}$.

Thus, the parity conservation $P = P_i$ or $(-1)^{J} = (-1)^{l_i+0+\lambda_i}$ constrains the initial channels that allow $\bar{\mathrm{H}}^{+}$ production reaction (3). The channels α are specified by the fragments and their angular momentum of relative motion λ (or λ_i). Distinguishing the kinds of the fragments by $\mathcal{F}$, we list the channels α that lead to the $\bar{\mathrm{H}}^{+}$ production in Table 1. As an example, in the case of $J = 2$, the angular momentum of the relative motion of $\mathrm{Ps}(ns) + \bar{\mathrm{H}}(1s)$ is constrained to be $\lambda_i = 2$. The same constraints for $\mathrm{Ps}(np) + \bar{\mathrm{H}}(1s)$ result in $\lambda_i = 1, 3$ for $J = 2$ because $|J - 1| \leq \lambda_i \leq J + 1$ and $(-1)^{J} = (-1)^{1+0+\lambda_i}$. Turning to the case of the $\mathrm{Ps}(3d) + \bar{\mathrm{H}}(1s)$ channel in $J = 2$, only the $\lambda_i = 0, 2, 4$ are allowed by $|J - 2| \leq \lambda_i \leq J + 2$ and $(-1)^{J} = (-1)^{2+0+\lambda_i}$.
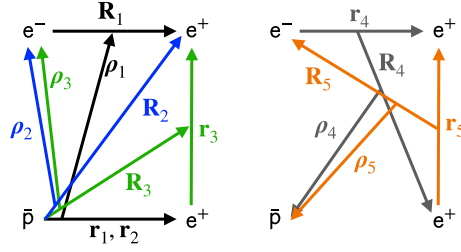
Fig. 1 Jacobi coordinate sets that are used in the present calculation. All sets are used simultaneously in the description of the multichannel scattering wave function, in order to assure the adequate description of correlation in the reaction region and the proper asymptotic behavior of the fragments

We construct $\{\Phi_\upsilon\}$ using a Gaussian expansion method (GEM) [55–57], in terms of radial Gaussian functions and spherical harmonics as

$$
\Phi_\upsilon = \sum_{c=1}^{5} \sum_{l_c L_c \lambda_c} \sum_{n_c N_c \upsilon_c} A^{(\upsilon)}_{c n_c N_c \upsilon_c l_c L_c \lambda_c} \left\{ r_c^{l_c} R_c^{L_c} \rho_c^{\lambda_c} \exp\left(-\frac{r_c^2}{r_{n_c}^2} - \frac{R_c^2}{R_{N_c}^2} - \frac{\rho_c^2}{\rho_{\upsilon_c}^2} \right) \right.
$$
$$
\left. \times \left[\left[Y_{l_c}(\hat{\mathbf{r}}_c) Y_{L_c}(\hat{\mathbf{R}}_c) \right]_{\Lambda_c} Y_{\lambda_c}(\hat{\boldsymbol{\rho}}_c) \right]_{JM} + (1 \leftrightarrow 2) \right\}, \tag{8}
$$

where the sets of Jacobi coordinates $\{\mathbf{r}_c, \mathbf{R}_c, \boldsymbol{\rho}_c\}$ are shown in Fig. 1. The first coordinate set $c = 1$ is suitable to describe four-body interactions of Ps + $\bar{\text{H}}$ configuration and $c = 2$ and $c = 3$ are suitable to describe the interactions of $e^- + \bar{\text{H}}^+$ configuration. The linear coefficients $A^{(\upsilon)}_{c n_c N_c \upsilon_c l_c L_c \lambda_c}$ are determined by the diagonalization of the Hamiltonian H with Φ. Non-linear coefficients $\{r_{n_c}\}$, $\{R_{N_c}\}$ and $\{\rho_{\upsilon_c}\}$ are chosen in accordance with geometrical progression. The total number of basis functions used for the expansion is denoted as n_b.

The use of the basis functions written in several coordinate systems facilitates the description of the four-body interactions and multi-channel character of the scattering. $\{\Phi_\upsilon\}$ provides the explicit description of virtual $\bar{\text{H}}$ excitation, virtual Ps excitation, virtual Ps^+ formation (mainly described by $c = 4, 5$ coordinate sets in Fig. 1) and transient formation of $\bar{\text{H}}^+$ and the resonances of $\bar{\text{H}}$Ps during the scattering. They describe also the mutual polarization of the atoms which is important in the description of their collisional interaction.

The Schrödinger equation (5) is then converted to a set of coupled equations with the following conditions,

$$
\langle \psi_\alpha / \mathcal{R}_\alpha(\rho_c) | H - E | \Psi \rangle_{\mathbf{r}_c, \mathbf{R}_c, \hat{\boldsymbol{\rho}}_c} = 0, \tag{9}
$$

and

$$
\langle \Phi_\upsilon | H - E | \Psi \rangle = 0. \tag{10}
$$

Here, $\langle \cdots \rangle_{\mathbf{r}_c, \mathbf{R}_c, \hat{\boldsymbol{\rho}}_c}$ means the integration over the indicated coordinates leaving out integration over ρ_c. $\mathcal{R}_\alpha(\rho_c)$ is the part of the channel function ψ_α, it describes the relative motion of the fragments in the open channels α. We solve it using a compact finite difference method [58] under proper boundary conditions at $\rho_c \to \infty$, and extract scattering matrix elements $S^{(JM)}_{\alpha \alpha_i}$.
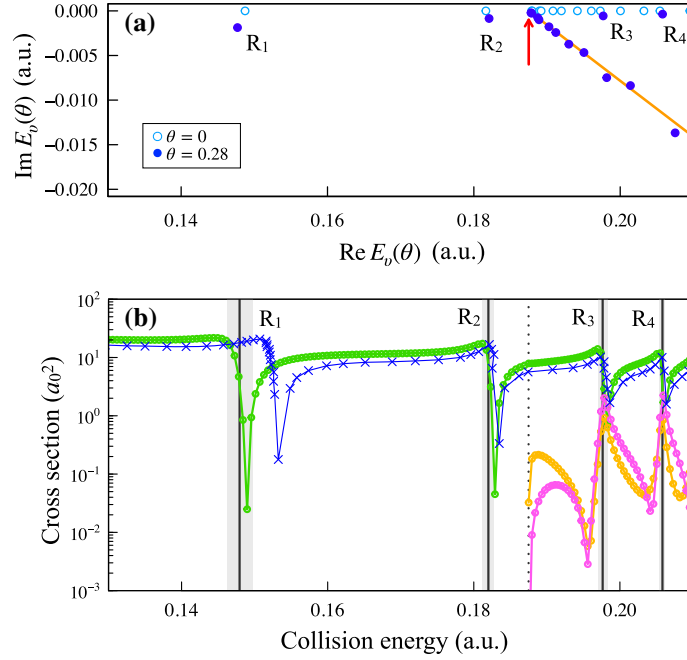
Cross sections from an open channel α_i to another open channel α are given by

$$
\sigma^{(JM)}_{\alpha \alpha_i} = \frac{\pi}{k_{\alpha_i}^2} |\delta_{\alpha \alpha_i} - S^{(JM)}_{\alpha \alpha_i}|^2. \tag{11}
$$

Since the initial wave involves all partial waves, the scattering cross section from $\mathcal{F}_i$ to $\mathcal{F}$ can be expressed as

$$
\sigma_{\mathcal{F} \mathcal{F}_i} = \sum_{\lambda_i} \frac{1}{(2l+1)(2L+1)} \sum_{J} \sum_{\alpha, \alpha_i} (2J+1) \sigma^{(JM)}_{\alpha \alpha_i}. \tag{12}
$$

Note that the allowed α_i should be compatible with λ_i with regard to the addition and conservation of angular momenta.

Fig. 2 Upper panel: example of a complex coordinate rotation calculation where the blue symbols (circles and dots) represent the eigenvalues for the two indicated scaling angles (unscaled and scaled calculations, respectively). The arrow shows the threshold energy for $n = 2$ excited Ps. R_1, R_2, R_3 and R_4 are complex energies representing resonances. Lower panel: scattering cross sections, green: elastic, orange: excitation of Ps to $2s$, and pink: excitation of Ps to $2p$. The resonances are clearly visible as abrupt changes in the cross sections. We note that the resonances in the inelastic and elastic scattering have the same energy but different shapes. The vertical dotted line indicates the threshold energy for $n = 2$ excited Ps. Resonance energies and the widths that are obtained in the complex coordinate rotation calculation are indicated by the vertical solid lines and the shades. The blue cross symbols represent results of the close-coupling calculation [34]

3 Results and Discussion

We first investigate the resonant scattering (4) in Ps($1s$)-$\bar{\text{H}}$($1s$) s-wave collision (hence, $J = 0$), reviewing our previous calculation [47]. Complex coordinate rotation calculations have predicted several resonance states $[\text{e}^-; \bar{\text{H}}^+]$ that converge to the $\text{e}^- + \bar{\text{H}}^+$ threshold energy [47,59,60]. These resonance states can be analysed by a quantum defect theory [59], and are attributed to a series of Rydberg states of the electron associated with $\bar{\text{H}}^+$. Two of these resonance states are located below the first excitation threshold energy of Ps, and the other are located above.

The resonance energies E_r and widths Γ can be calculated by the complex coordinate rotation method [61]. Since $\{\Phi_\upsilon\}$ are spanned in terms of square integrable basis function, we have

$$\left\langle \overline{\Phi_{\upsilon'}(\theta)} \middle| U(\theta) H U^{-1}(\theta) \middle| \Phi_\upsilon(\theta) \right\rangle = E_\upsilon(\theta)\delta_{\upsilon\upsilon'}, \tag{13}$$

where $U(\theta)$ is a complex dilation operator, $U(\theta)r = e^{i\theta}r$.

Figure 2a shows the eigenenergies $\{E_\upsilon(\theta = 0)\}$ and $\{E_\upsilon(\theta = 0.28\,\text{rad})\}$ that are obtained by solving the complex dilated eigenvalue problem. $\{\Phi_\upsilon\}$ are expanded in terms of $n_\text{b} = 38320$ basis functions. Two eigenenergies of $\{E_\upsilon(\theta = 0.28\,\text{rad})\}$ below the Ps($n = 2$) threshold energy are found close to those of $\{E_\upsilon(\theta = 0)\}$. We call these resonances R_1 and R_2. Their resonance energies and widths are ($E_r = 0.1479$, $\Gamma = 0.0035$) and ($E_r = 0.1820$, $\Gamma = 0.0016$), respectively. While most of the complex eigenvalues $\{E_\upsilon(\theta = 0.28\,\text{rad})\}$ above the Ps($n = 2$) excitation threshold energy are rotated downward by an angle 2θ as illustrated by the orange line, two of them do not follow the outrotation and are independent of the rotation angle. These additional resonances are called R_3 and R_4, and their resonance energies and widths are determined as ($E_r = 0.1976$, $\Gamma = 0.0013$) and ($E_r = 0.2058$, $\Gamma = 0.0007$), respectively.

Figure 2b shows the elastic and inelastic cross sections of Ps($1s$)-$\bar{\text{H}}$($1s$) s-wave collision in the vicinity of the Ps($n = 2$) excitation threshold energy. In this energy region, the open fragment channels are $\mathcal{F} = 1, 2$ and 3 ($\alpha = 1, 2$ and 3). The convergence of these cross sections against the number of four-body functions $\upsilon_{\max}$
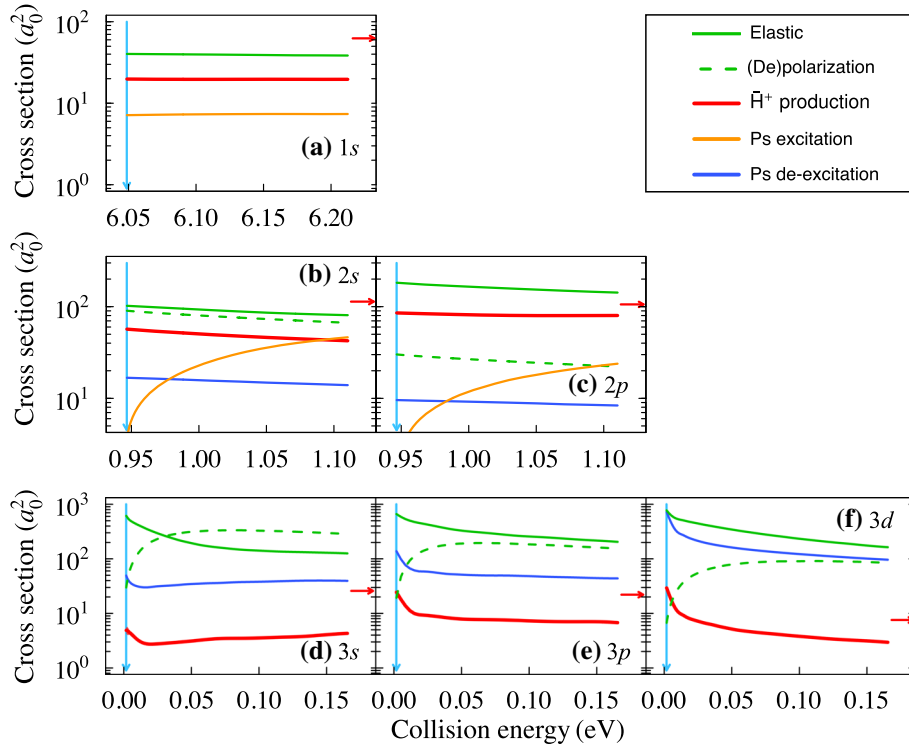
Fig. 3 Elastic and inelastic scattering cross sections $\sigma_{\mathcal{F}\mathcal{F}_i}$ for Ps(nl) + $\bar{\text{H}}$(1s) collisions in positronic spin singlet state are displayed. $\bar{\text{H}}^+$ production cross section (red lines) are compared with the latest improved CDW-FS results [53] (indicated by the right-head arrows because the energy scales that the CDW-FS deal with are different from the present work). The light-blue vertical arrows indicate the threshold energies of $\bar{\text{H}}^+$ production in our calculation

included in the expansion of Eq. (6) (and also against the number of basis functions n_b) was investigated in Ref. [47], and $\upsilon_{\max} \geq 28$ gives converged cross sections. Below the Ps($n = 2$) excitation threshold energy, the elastic cross sections show two dips corresponding to the resonances R_1 and R_2. At the threshold energy, the inelastic scattering cross sections grow from zero, which is consistent with the Wigner's threshold law that predicts that the excitation cross sections should grow in proportion to $k_f^{2\lambda_f+1}$. We can see additional two dips in elastic cross sections and peaks of inelastic cross sections above the threshold energy. These dips and peaks correspond to the resonance energy predicted by the complex coordinate rotation calculation. Due to the coupling with the background phase shifts, the cross sections show asymmetric behavior around the resonance energy [46].

The importance of explicit description of $\bar{\text{H}}^+$ formation during the resonant scattering has been pointed out in close-coupling investigation [34]. As shown by the blue crosses in Fig. 2b, our elastic scattering cross sections agree well with the close-coupling results, except for the neighborhood of the lowest resonance. We believe that the shift in the position of the R_1 resonance comes from the more correct description of the $\bar{\text{H}}^+$-e^- system. The lowest resonance is the one which deviates the most from the frozen core description of the $\bar{\text{H}}^+$-e^- system used in Ref [34]. Since the functions Φ_υ are obtained by the diagonalization of the four-body Hamiltonian, they can offer more precise description of the $\bar{\text{H}}^+$-e^- interaction (particularly because of the use of dedicated sets of Jacobi coordinates) than the use of frozen three-body wavefunction of $\bar{\text{H}}^+$ (which was not very precise). In addition, the present calculation gives both elastic and inelastic cross sections within the same calculation of the S-matrix, which, through the analysis of the S-matrix elements, provides information about the branching ratios in the decay of resonant states.

We calculate $\sigma_{\alpha\alpha_i}^{(JM)}$ for each $0 \leq J \leq 2$ for Ps($n = 3$), $0 \leq J \leq 6$ for Ps($n = 2$) and $0 \leq J \leq 4$ for Ps($n = 1$), and subsequently construct $\sigma_{\mathcal{F}\mathcal{F}_i}$. We display the $\bar{\text{H}}^+$ production cross sections together with elastic/inelastic scattering cross sections in Fig. 3. The $\bar{\text{H}}^+$ production (rearrangement) cross section is defined

as

$$\sigma_{\text{rearr}}(1 \leq \mathcal{F}_i \leq 6) = \sigma_{7\mathcal{F}_i}. \tag{14}$$

To better reflect the overall outcome of the scattering and to simplify the presentation, other inelastic channel-to-channel cross sections $\sigma_{\mathcal{F}\mathcal{F}_i}$ that contribute to the same type of process are summed together according to the following:

$$\sigma_{\text{ex}}(\mathcal{F}_i = 1) = \sum_{2 \leq \mathcal{F} \leq 6} \sigma_{\mathcal{F}\mathcal{F}_i}, \tag{15}$$

$$\sigma_{\text{ex}}(\mathcal{F}_i = 2, 3) = \sum_{4 \leq \mathcal{F} \leq 6} \sigma_{\mathcal{F}\mathcal{F}_i}, \tag{16}$$

$$\sigma_{\text{dex}}(\mathcal{F}_i = 2, 3) = \sum_{\mathcal{F}=1} \sigma_{\mathcal{F}\mathcal{F}_i}, \tag{17}$$

$$\sigma_{\text{dex}}(\mathcal{F}_i = 4, 5, 6) = \sum_{1 \leq \mathcal{F} \leq 3} \sigma_{\mathcal{F}\mathcal{F}_i}, \tag{18}$$

$$\sigma_{\text{pol}}(\mathcal{F}_i = 2) = \sum_{\mathcal{F}=3} \sigma_{\mathcal{F}\mathcal{F}_i}, \tag{19}$$

$$\sigma_{\text{pol}}(\mathcal{F}_i = 3) = \sum_{\mathcal{F}=2} \sigma_{\mathcal{F}\mathcal{F}_i}, \tag{20}$$

$$\sigma_{\text{pol}}(\mathcal{F}_i = 4) = \sum_{\mathcal{F}=5,6} \sigma_{\mathcal{F}\mathcal{F}_i}, \tag{21}$$

$$\sigma_{\text{pol}}(\mathcal{F}_i = 5) = \sum_{\mathcal{F}=4,6} \sigma_{\mathcal{F}\mathcal{F}_i}, \tag{22}$$

and

$$\sigma_{\text{pol}}(\mathcal{F}_i = 6) = \sum_{\mathcal{F}=4,5} \sigma_{\mathcal{F}\mathcal{F}_i}, \tag{23}$$

where σ_{ex} are Ps excitation cross sections, σ_{dex} Ps deexcitation cross sections, σ_{pol} Ps (de)polarization cross sections associated with a change of internal orbital angular momentum of Ps without a change of its principal quantum number.

The above cross sections are presented in Fig. 3 as a function of the collision energy E_i. Each panel shows cross sections for all scattering processes (elastic, inelastic and rearrangement) originating from the same initial state of Ps(nl). For comparison, we indicate also the values of the recent improved CDW-FS calculation read from the Ref. [53].

For Ps($1s$) + $\bar{\text{H}}$($1s$) collisions ($\mathcal{F}_i = 1$), as shown in Fig. 3a, the $\bar{\text{H}}^+$ production channel, which opens at 6.0486 eV, is the second dominant process after the elastic scattering. In the present energy region, these cross sections are nearly constant. The σ_{rearr} starts at the finite value and is also constant in agreement with Wigner's threshold law [62] for the case of the Coulomb attractive final fragments. The CDW-FS calculation predicts cross sections that are several times higher in comparison to the present calculation. This is not surprising because the CDW-FS method is not expected to perform well in the near-threshold region.

Figure 3b, c show the results of Ps($n = 2$) + $\bar{\text{H}}$($1s$) collisions ($\mathcal{F}_i = 2, 3$). σ_{rearr} is finite at the threshold energy. Like the Ps($1s$) collision, Ps($n = 2$) + $\bar{\text{H}}$($1s$) collisions produce $\bar{\text{H}}^+$ as the dominating inelastic scattering process. Similarly to the case of $\mathcal{F}_i = 1$, the CDW-FS calculation predicts slightly higher cross sections than the present calculation at the threshold energy.

In collisions between Ps($n = 3$) and $\bar{\text{H}}$($1s$) ($\mathcal{F}_i = 4, 5, 6$), as shown in Fig. 3d–f, σ_{rearr} decreases above the threshold energy, and then is nearly constant at higher energies. σ_{dex} obey the Wigner's threshold law [62] for the neutral fragments, varying in proportion to $E_i^{\lambda_i - 1/2}$, and thus for all l, σ_{dex} is finite at the threshold of $\bar{\text{H}}^+$ formation ($E_i = 0.0017$ eV). The CDW-FS for Ps($3s$) collisions predicts slightly higher cross sections than obtained in the present calculation while for the Ps($3p, 3d$) collisions the CDW-FS cross sections are of a similar order of magnitude as the ones presented here.

In addition to the absolute value of the cross sections, the comparison of the rearrangement originating from different l states of Ps(nl) is of interest. At the threshold energy, Ps($2p$) collision shows larger σ_{rearr} than Ps($2s$) collision. Similarly, Ps($3d/3p$) collisions show larger σ_{rearr} than Ps($3s$) collision. On the other hand, the CDW-FS calculation predicts the largest σ_{rearr} in Ps($2s$) and Ps($3s$) collisions, respectively. These discrepancies might be of experimental importance. Most probably they arise due to the perturbative treatment inherent to the CDW-FS method, which nevertheless performs surprisingly well.

4 Conclusion

We have reviewed our four-body calculations of Ps(nl) + $\bar{\mathrm{H}}$($1s$) scattering for $n \leq 3$. Our method combines the four-body structure calculation (implemented in the Gaussian basis) with the coupled channel procedure. The calculation includes all open channels in the energy range that starts at the first inelastic threshold (Ps($n = 2$) + $\bar{\mathrm{H}}$($1s$)) and extends beyond the threshold for the rearrangement to $\bar{\mathrm{H}}^+$ + e$^-$.

The cross sections are presented throughout a Rydberg-like series of resonances converging to the threshold energy for the ionic core ($\bar{\mathrm{H}}^+$). These cross sections show typical resonant shapes (abrupt peaks and dips of Breit-Wigner type) characteristic for the elastic scattering in the presence of inelastic and background scattering. These features are gradually blurred as the resonances cease to be isolated towards the threshold for formation of $\bar{\mathrm{H}}^+$. The energy positions of the resonant profiles are in good agreement with the resonance energies that we have calculated using the complex coordinate rotation method.

$\bar{\mathrm{H}}^+$ production cross sections near the threshold energy are determined together with the cross sections for all competing elastic/inelastic processes. A comparison with the latest improved CDW-FS calculation is reported.

References

1. M. Amoretti et al., Nature **419**, 456 (2002)
2. Y. Enomoto et al., Phys. Rev. Lett. **105**, 243401 (2010)
3. The ALPHA Collaboration, Nat. Phys. **7**, 558 (2011)
4. N. Kuroda et al., Nat. Commun. **5**, 4089 (2014)
5. E. Widmann et al., Hyperfine Interact. **240**, 5 (2018)
6. B. Kolbinger et al., EPJ Web Conf. **181**, 01003 (2018)
7. C. Malbrunot et al., Philos. Trans. R. Soc. A **376**, 20170273 (2018)
8. M. Ahmadi et al., Nature **557**, 71 (2018)
9. M. Ahmadi et al., Nature **541**, 506 (2016)
10. M. Ahmadi et al., Nature **548**, 66 (2017)
11. M. Ahmadi et al., Nature **561**, 211 (2018)
12. C.L. Cesar et al., AIP Conf. Proc. **770**, 33 (2005)
13. The ALPHA Collaboration, C. Amole, et al., Nature Commun. **4**, 1785 (2013)
14. P. Indelicato et al., Hyperfine Interact. **228**, 141 (2014)
15. P. Pérez et al., Hyperfine Interact. **233**, 21 (2015)
16. P. Pérez, Y. Sacquin, Classical Quant. Grav. **29**, 184008 (2012)
17. Y. Sacquin, Eur. Phys. J. D **68**, 31 (2014)
18. A. Kellerbauer et al., Nucl. Instrum. Meth. Phys. Res. B **266**, 351 (2008)
19. P. Scampoli, J. Storey, Mod. Phys. Lett. A **29**, 1430017 (2014)
20. A. Knecht et al., Hyperfine Interact. **228**, 121 (2014)
21. M. Kimura et al., J. Phys.: Conf. Ser. **631**, 012047 (2015)
22. C. Evans et al., EPJ Web Conf. **182**, 02040 (2018)
23. C. Amsler et al., Commun. Phys. **4**, 19 (2021)
24. M.T. McAlinden, F.G.R.S. MacDonald, H.R.J. Walters, Can. J. Phys. **74**, 434 (1996)
25. S.K. Adhikari, Nucl. Instrum. Methods Phys. Res. B **192**, 74 (2002)
26. I.I. Fabrikant, G.F. Gribakin, Phys. Rev. A **90**, 052717 (2014)
27. I.I. Fabrikant, G.F. Gribakin, Phys. Rev. Lett. **112**, 243201 (2014)
28. R.S. Wilde, I.I. Fabrikant, J. Phys.: Conf. Ser. **1412**, 052011 (2020)
29. R.J. Drachman, S.K. Houston, Phys. Rev. A **14**, 894 (1976)
30. S.K. Adhikari, P. Mandal, J. Phys. B: At. Mol. Opt. Phys. **33**, L761 (2000)
31. S.K. Adhikari, Phys. Rev. A **63**, 054502 (2001)

32. S.K. Adhikari, P. Mandal, J. Phys. B: At. Mol. Opt. Phys. **34**, L187 (2001)
33. P.K. Biswas, J. Phys. B: At. Mol. Opt. Phys. **34**, 4831 (2001)
34. J.E. Blackwood, M.T. McAlinden, H.R.J. Walters, Phys. Rev. A **65**, 030502 (2002)
35. I.A. Ivanov, J. Mitroy, K. Varga, Phys. Rev. A **65**, 032703 (2002)
36. P.V. Reeth, J.W. Humberston, J. Phys. B: At. Mol. Opt. Phys. **36**, 1923 (2003)
37. J.Y. Zhang, J. Mitroy, Phys. Rev. A **78**, 012703 (2008)
38. D. Woods, S.J. Ward, P. Van Reeth, Phys. Rev. A **92**, 022713 (2015)
39. M.S. Wu, J.Y. Zhang, Y. Qian, K. Varga, U. Schwingenschlögl, Z.C. Yan, Phys. Rev. A **103**, 022817 (2021)
40. S.J. Brawley, S. Armitage, J. Beale, D.E. Leslie, A.I. Williams, G. Laricchia, Science **330**, 789 (2010)
41. R.S. Wilde, I.I. Fabrikant, Phys. Rev. A **97**, 052708 (2018)
42. J.Y. Zhang, M.S. Wu, Y. Qian, X. Gao, Y.J. Yang, K. Varga, Z.C. Yan, U. Schwingenschlögl, Phys. Rev. A **100**, 032701 (2019)
43. M.S. Wu, J.Y. Zhang, X. Gao, Y. Qian, H.H. Xie, K. Varga, Z.C. Yan, U. Schwingenschlögl, Phys. Rev. A **101**, 042705 (2020)
44. A.R. Swann, D.B. Cassidy, A. Deller, G.F. Gribakin, Phys. Rev. A **93**, 052712 (2016)
45. S. Roy, R. Biswas, C. Sinha, Phys. Rev. A **71**, 044701 (2005)
46. P. Froelich, T. Yamashita, Y. Kino, S. Jonsell, E. Hiyama, K. Piszczatowski, Hyperfine Interact. **240**, 46 (2019)
47. T. Yamashita, Y. Kino, E. Hiyama, K. Piszczatowski, S. Jonsell, P. Froelich, JJAP Conf. Proc. (accepted)
48. T. Yamashita, Y. Kino, E. Hiyama, K. Piszczatowski, S. Jonsell, P. Froelich, J. Phys.: Conf. Ser. **1412**, 052012 (2020)
49. T. Yamashita, Y. Kino, E. Hiyama, S. Jonsell, P. Froelich, New J. Phys. **23**, 012001 (2021)
50. P. Comini, P.A. Hervieux, New J. Phys. **15**, 095022 (2013)
51. P. Comini, P.A. Hervieux, J. Phys.: Conf. Ser. **443**, 012007 (2013)
52. P. Comini, P.A. Hervieux, F. Biraben, Hyperfine Interact. **228**, 159 (2014)
53. P. Comini, P.A. Hervieux, K. Lévêque-Simon, New J. Phys. **23**, 029501 (2021)
54. R.G. Newton, *Scattering Theory of Waves and Particles* (Springer, New York, 1982)
55. E. Hiyama, Y. Kino, M. Kamimura, Prog. Part. Nucl. Phys. **51**, 223 (2003)
56. E. Hiyama, Prog. Theo. Exp. Phys. **2012** (2012)
57. E. Hiyama, M. Kamimura, Front. Phys. **13**, 132106 (2018)
58. J. Zhao, R.M. Corless, Appl. Math. Comput. **177**, 271 (2006)
59. Z.C. Yan, Y.K. Ho, Phys. Rev. A **84**, 034503 (2011)
60. J.E. Blackwood, M.T. McAlinden, H.R.J. Walters, Phys. Rev. A **65**, 032517 (2002)
61. Y. Ho, Phys. Rep. **99**, 1 (1983)
62. E.P. Wigner, Phys. Rev. **73**, 1002 (1948)